The Korean Journal of Ceramics, **4** [2] 103 - 113 (1998)

Use of High-Temperature Gas-Tight Electrochemical Cells to Measure Electronic Transport and Thermodynamics in Metal Oxides

Jong-Hee Park, Beihai Ma and Eun Tae Park

Energy Technology Division, Argonne National Laboratory, Argonne, IL 60439 U. S. A

(Received October 2, 1997)

By using a gas-tight electrochemical cell, we can perform high-temperature coulometric titration and measure electronic transport properties to determine the electronic defect structure of metal oxides. This technique reduces the time and expense required for conventional thermogravimetric measurements The components of the gas-tight coulometric titration cell are an oxygen sensor, Pt/yttria stabilized zirconia (YSZ)/Pt, and an encapsulated metal oxide sample. Based on cell design, both transport and thermodynamic measurements can be performed over a wide range of oxygen partial pressures ($pO_2=10^{-35}$ to 1 atm). This paper describes the high-temperature gas-tight electrochemical cells used to determine electronic defect structures and transport properties for pure and doped-oxide systems, such as YSZ, doped and pure ceria (Ca-CeO_2 and CeO_2), copper oxides and copper-oxide-based ceramic superconductors, transition metal oxides, $SrFeCo_{0.5}O_x$, and $BaTiO_3$.

Key words : Mobility of holes, Mobility of electrons, Ceria (CeO_2), Gas-tight electrochemical cell, Optical gap (E_g), YSZ (Yttria Stabilized Zirconia)

I. Introduction

The value of directly obtaining partial molar thermodynamic quantities in the investigation of nonstoichiometric oxides is that it allows thermodynamic characterization without assuming a particular defect model. These quantities, which consist mainly of variations in oxygen chemical potential with changing temperature and composition, can best be used in support of, and in conjunction with, a proposed defect model. Together, they provide insight, understanding, and a concise description of the nonstoichiometric behavior to develop various sensors and membranes for the application of gas separation or synthesis for industry.

Of the many different measurement systems that have been used in high-temperature thermodynamic studies of metal oxides, electrochemical titration cells, which incorporate solid electrolytes, offer the greatest versatility. In previous studies of metal oxides (e.g., CeO_{2-x}), electron mobility (μ) was determined by combining separate experimental measurements of deviation from stoichiometry (x) and electrical conductivity (σ). A coulometric titration technique, which extends the utility of the titration cell to include the direct and simultaneous measurements of thermodynamic quantities and electronic conductivity, is presented. To perform the high-temperature coulometric titration technique, we must understand the nonstoichiometric defect behavior in yttria stabilized zirconia (YSZ). Therefore YSZ and nonstoichiometric cerium dioxide were chosen for the purpose of demonstration.

When a metal oxide (binary, ternary, or even quaternary oxides, in which M, N, L are different nonvolatile metals), designated as $M(NL)O_2$, is in equilibrium with the surrounding oxygen atmosphere at elevated temperatures, we may write the overall reaction as (only "M" is denoted for convenience)

$$MO_2(s)=MO_{2-x}(s)+\frac{x}{2}O_2(g) \tag{1}$$

where x indicates the deviation from stoichiometry. According to the Gibbs phase rule, two intrinsic parameters are needed to describe the x values, i.e., temperature and pO_2; thus, $x=x(T, pO_2)$.

1. Defects in yttria-stabilized zirconia (YSZ)

YSZ has a stable fluorite cubic structure consisting of Zr^{+4} at outer face centered-cubic positions and O^{-2} at inner simple-cubic positions. Because the proposed defect model in metal oxide systems is similar, YSZ was chosen for the demonstration.

When ZrO_2 is doped with Y_2O_3, a doubly ionized oxygen vacancy ($V_O^{\cdot\cdot}$) is produced. The defect reaction can be represented as[1]

$$YO_{1.5}\rightarrow Y'_{Zr}+\frac{1}{2}V_O^{\cdot\cdot}+\frac{3}{2}O_O^x, \tag{2}$$

where Y'_{Zr} indicates yttrium on the zirconium site with an effective charge of -1, and O_O^x indicates normal oxygen on an oxygen site.

The formula for YSZ containing y moles of yttria is

$Zr_{1-y}Y_yO_{2-y/2}$. The electroneutrality condition is[2]

$$[Y'_{Zr}]=2[V_O^{\cdot}] \tag{3}$$

where the bracket indicates the concentration of each species. When the YSZ is in equilibrium with the surrounding oxygen, the overall solid/gas reaction is

$$Zr_{1-y}Y_yO_{2-\frac{y}{2}}=Zr_{1-y}Y_yO_{2-\frac{y}{2}-x}+\frac{x}{2}O_2(g) \tag{4}$$

The nonstoichiometric defect reactions proposed by several authors[1-4] for an n-type region, i.e., at low oxygen pressure, with an enthalpy of ΔH^0 are

$$2Zr_{Zr}^x+O_O^x=2Zr'_{Zr}+V_O^{\cdot\cdot}+\frac{1}{2}O_2(g) \tag{5a}$$

or simply,

$$O_O^x \rightarrow V_O^{\cdot\cdot}+2e'+\frac{1}{2}O_2(g), \tag{5b}$$

where Zr'_{Zr} indicates a localized electron on a zirconium site. Because of the nonstoichiometric defect reaction, the electroneutrality equation (Eq. 3) becomes

$$2[V_O^{\cdot\cdot}]=[Zr'_{Zr}]+[Y'_{Zr}] \tag{6}$$

The site fractions of localized electrons and yttrium atoms on zirconium sites may be expressed in terms of x and y as

$$[Zr'_{Zr}]=2x$$

and (7)

$$[V_O^{\cdot\cdot}]=\frac{x+y}{2}$$

The mass action constant, K_{ma}, associated with the defect reaction, (Eq. 5a) is

$$K_{ma}=\frac{[Zr'_{Zr}]^2[V_O^{\cdot\cdot}]}{[Zr_{Zr}^x]^2[O_O^x]}\,pO_2^{1/2} \tag{8}$$

On the basis of Eq. 7 and the assumption that $[Zr_{Zr}^x]=1-y$ and $[O_O^x]=1-(y/2)$, then K_{ma} can be written as

$$K_{ma}=\frac{(2x)^2[(x+y)/2]}{(1-y)[1-(y/2)]}\,pO_2^{1/2} \tag{9}$$

By differentiating and rearranging Eq. 9, we obtain

$$\frac{\partial\log(pO_2)}{\partial\log(x)}=-4-\frac{2x}{x+y} \tag{10}$$

When y=0.148 (8 mole % YSZ) and y>>x, the slope is essentially -4. For pure oxide (no doping), i.e., y=0, Eq. 10 becomes $\partial\log(pO_2)/\partial\log(x)=-6$. For ZrO_2 doped with 8 mole % YSZ, the deviation from stoichiometry, x, is

$$x=KpO_2^{-1/4} \tag{11}$$

where the proportionality constant $K=2.73\sqrt{K_{ma}}$. Using the thermodynamic relation $\Delta H^o=\Delta G^o+T\Delta S^o$, we may also write

$$K_{ma}\propto\exp\left(\frac{-\Delta G^0}{kT}\right)=\exp\left(\frac{\Delta S^0}{k}\right)\exp\left(\frac{-\Delta H^0}{kT}\right) \tag{12}$$

The reaction for the formation of oxygen is

$$O_2(1\ atm, g)+4Zr'_{Zr}+2V_O^{\cdot\cdot}=4Zr_{Zr}^x+2O_O^x \tag{13}$$

with an enthalpy of ΔH_{O_2}. From Eqs. 5 and 13, it is apparent that

$$\Delta H_{O_2}=-2\Delta H^o \tag{14}$$

When we plot the log K vs. 1/T or log x (fixed pO_2) vs. 1/T, $-\Delta H^o=2k$ (Boltzman constant) times the slope, and therefore, ΔH_{O_2} can be obtained from 4k times the slope.

2. Solid-state coulometric titration

High-temperature solid-state coulometric titration of oxide systems involves the removal or addition of oxygen by means of an oxygen pump. During pumping, the solid-gas reaction is represented as[3,4]

$$MO_2(s)\underset{\text{pump-in}}{\overset{\text{pump-out}}{\Leftrightarrow}}MO_{2-x}(s)+\frac{x}{2}O_2(g) \tag{15}$$

As oxygen is pumped out of the cell (and therefore out of the specimen), one can measure the EMF, which corresponds to the equilibrium pO_2 for the sample and gas. The gas-tight chamber incorporates an electrochemical sensor that also serves as an oxygen pump and allows for the simultaneous control of oxygen flux and measurement of oxygen potential. When pumping oxygen, two primary sources of oxygen are considered : (a) the gas phase in the cell and (b) the sample phase, which is described by Eq. 15. The total moles of oxygen pumped are denoted by Δn_{O_2}, which can be evaluated by Faraday's law:

$$\Delta n_{O_2}=\frac{i\Delta t}{4F}=\Delta n_{O_2(gas)}+\Delta n_{O_2(specimen)} \tag{16}$$

where $\Delta n_{O_2(gas)}$ and $\Delta n_{O_2(specimen)}$ are the moles of oxygen pumped from the gas and specimen, respectively. To calculate the net amount of oxygen removed from the specimen, we must subtract the gas-phase contribution from the total amount of oxygen. When the gas phase is treated as an ideal gas,

$$\Delta n_{O_2(gas)}=\frac{V}{RT}\Delta pO_2, \tag{17}$$

where V is the free volume of the gas-tight chamber, $\Delta pO_2=pO_{2,f}-pO_{2,i}$, and the subscripts f and i are the final and initial equilibrium pO_2. For the specimen,

$$\Delta n_{O_2(specimen)}=\frac{W}{2M}[x_f-x_i] \tag{18}$$

where W is the weight of the specimen, M is the molecular weight, and x_f and x_i are the equilibrium x values for a given pO_2. However, when $\Delta n_{O_2(gas)}$ is small enough in comparison to $\Delta n_{O_2(specimen)}$, the thermodynamic behavior

of the system is essentially due to the solid sample.[3] If we can choose by analogy with Eq. 11,

$$x_f = K p O_{2,f}^{-1/4}$$

and (19)

$$x_i = K p O_{2,i}^{-1/4},$$

where the proportionality constant K is the value at pO_2= 1.0 atm. The difference between these two states is

$$\Delta x = x_f - x_i = K[pO_{2,f}^{-1/4} - pO_{2,i}^{-1/4}] = K\Delta pO_2^{-1/4} \quad (20)$$

and the proportionality constant K can be determined from Eq. 20.[20]

3. Constant-composition measurement

In a gas-tight cell at low oxygen pressures, the thermodynamics of the system are essentially determined by the solid sample.[3] In this condition, we can apply the Gibbs-Helmholtz equation,[5]

$$\Delta H_{O_2} = \Delta G_{O_2} + T\Delta S_{O_2}, \quad (21)$$

where ΔG_{O_2}=-4FE, and $\Delta S_{O_2} = -(\partial \Delta G_{O_2}/\partial T)_{x=const} = 4F(\partial E/\partial T)_{x=const}$. Therefore,

$$\Delta H_{O_2} = -4FE + FT(\partial E/\partial T)_{x=const} = -4F[E - T(\partial E/\partial T)_{x=const}] \quad (22)$$

Thus, the relative partial molar enthalpy $\Delta\bar{H}_{O_2}$ and the relative partial molar entropy $\Delta\bar{S}_{O_2}$ can be determined from the changes in EMF with temperature at constant x; or from, respectively, the slope of log pO_2 vs. 1/T, i.e.,

$$\Delta\bar{H}_{O_2} = R[\partial \ln pO_2/\partial(1/T)]_{x=const} \quad (23)$$

and $\Delta\bar{S}_{O_2}$, the intercept at 1/T=0.

4. Electronic transport properties

The electronic conductivity (σ)

$$\sigma = nq\mu, \quad (24)$$

where n is the electron concentration, and μ the electron mobility. The mobility is expressed as

$$\mu = \mu_o \exp(-\frac{E_m}{kT}), \quad (25)$$

where μ_o is a pre-exponential constant, and E_m is the migration energy of electrons. In fluorite structures, the concentration of electrons (n) can be denoted as

$$n = \frac{8x}{a_o^3} \quad (26)$$

where a_o is the X-ray lattice parameter. By combining Eqs. 24-26, we obtain

$$\sigma = \frac{8x}{a_o^3} q\mu_o \exp(-\frac{E_m}{kT}) \quad (27)$$

5. Electrochemical transport

Heyne[6] derived the electrochemical transport equation for ambipolar transport in metal oxides under a chemical potential gradient

$$-j_e = j_i = (\sigma_i/4q) t_i t_e (\partial\mu_{O_2}/\partial x). \quad (28)$$

For ionic conductors, $t_i >> t_e$, i.e., $t_i \sim 1$, it gives

$$j_i = (\sigma_e/4q)(\partial\mu_{O_2}/\partial x). \quad (29)$$

For electronic conductors, $t_e >> t_i$, i.e., $t_e \sim 1$, it gives

$$j_i = (\sigma_i/4q)(\partial\mu_{O_2}/\partial x). \quad (30)$$

II. Experimental Approach

1. Experimental equipment

1.1 Electrochemical cell construction

Various designs of gas tight electrochemical cells are shown in Fig. 1. In Fig. 1a, two identical YSZ disks are used. The top disk of the cell serves as a permeation specimen and as an oxygen sensor. The bottom disk is primarily used as an oxygen pump. The walls of the cell consist of three 0.5-in.-diameter high-purity alumina (#998A, McDanel) rings that are separated from each other and the disks by thin Pyrex glass (#7740, Corning) rings. The alumina rings also provide high-temperature electrical insulation. Both YSZ disks were painted with platinum paste (code #6926 unfluxed, Engelhard) on the entire outer face and on that part of the inner face that would be within the enclosure. These electrodes were further prepared in air by several heating step, finally being fired at ≈980°C overnight. Platnum wires of 5 mil-diameter were used as electric leads in the Pyrex-sealed cell. The entire stack was placed in the measuring fur-

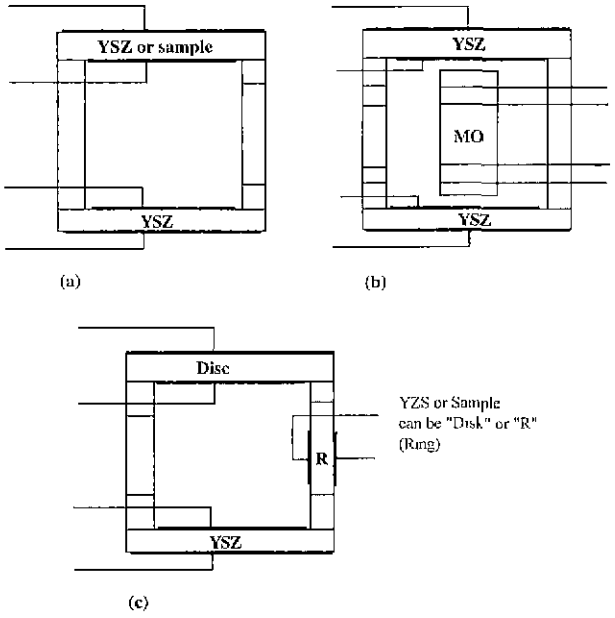

Fig. 1. Gas-tight coulometric titration cells that imclude the four-probe conductivity sample (a-c)

nace along a vertical axis and a spring force was applied to the stack. A 3% O_2/Ar gas mixture was passed through the system while firing up to 1000°C. During heating, the Pyrex glass (softening temperature 820°C) rings melted and provided a gas-tight seal. The limitation of mechanical pressure difference in the Pyrex seal was 0.35 atm at 920°C. This was determined by the continuous pumping in of oxygen through the electrolyte until failure. However, when the oxygen was pumped out from the inside cell, the maximum pressure obtainable was 0.03 atm because the initial gas mixture was 3% O_2-Ar. No problem in sealing was experienced when pumping oxygen out.

1.2 Four- probe conductivity cell

The various conductivity specimens were prepared by sintering. The final step was to cut the bar into a four-probe conductivity specimen and load it into the coulometric titration chamber shown in Fig. 1b. Both DC and AC conductivity can be measured; the AC conductivity was measured at a constant frequency of 1592 Hz.

1.3 Measuring assembly

The electrochemical cell was placed in an alumina tube of 3.8 cm outer diameter (OD). and 35 cm length, with a flat disc end. An open window measuring 2.5×5 cm was cut in the bottom of the alumina tube for installation of the electrochemical cell. This portion was sealed to the brass head with water-soluble high-temperature ceramic cement (Paste #1, Sauereisen Cement Co.) and then inserted into a quartz tube. The quartz (outer) tube was 36 cm in length and 4.5 cm in OD. It was connected to the brass head by an O-ring to form a gas-tight system. A spring-loaded alumina rod was loaded onto the cell stack to facilitate sealing. A thermocouple made of 16 mil Pt-13% Rh/Pt in a 6 mm OD thermocoupole tube was inserted into the 0.5-in. diameter alumina tube. A heat resistant alloy (Inconel) tube was placed in the furnace outside the measuring system. To protect it from electrical pickup, the alloy tube was grounded; serving as a heat sink, it also acts to provide a more uniform temperature.

2. Cell performance tests

To perform electrochemical transport measurements utilizing a Pyrex-glass-sealed gas-tight cell, the following preliminary tests were necessary.

2.1 Leak test by switching gas

After sealing the cell, the Pyrex seals by switching the gas outside of the cell from 3% O_2-Ar (original atmosphere) to O_2 (or air). If the seals are gas-tight the EMF should correlate with the oxygen potential difference within experimental error. If there are open pores or leakage is present, the indicating EMF will drop rapidly to zero after switching gas. The leak test was performed ≈900°C. The successful seals showed no significant change in EMF with time.

2.2 Cell volume Measurement by coulometric titration

The free volume of the electrochemical cell can be determined by coulometric titration. With the ideal gas law, PV=nRT, or $\Delta pO_2V=\Delta n_{O_2}RT$ when supplying current, $\Delta n_{O_2}=i \cdot t/4F$ and or, from the plot of pO_2 vs. time, t, the slope gives

$$\text{slope}=(\partial pO_2/\partial t)=(iRT/4F)/V \tag{31}$$

To determine the pO_2 range for which the above expressions are valid, a gas coulometric titration experiment was performed. The continuous pumping profile of pO_2 ranges form ≈0.2 atm to $\approx 10^{-6}$ atm at 982°C. Focusing on the pO_2 region of air (0.21 atm), we attempted several runs to determine volume by two approaches. For these experiments, an additional monitor (Fig. 1c) was added to the cell. The first approach utilized only one disc as an oxygen pump From a plot of pO_2 vs. time for this case one obtains a volume of 2.15 cm^3. In each case the average volume was within 0.5% of the individual runs.

2.3 Pumping performance tests

The above coulometric titration test can be used to accurately determine ionic transference numbers near 1. EMF or conductivity methods do not provide the accuracy obtainable by coulometric titration. The following experiments were carried out to determine the relative ionic transference number of various samples.

Using a three monitor cell (Fig. 1c), we evaluated the pumping performance of YSZ by supplying identical current to each of the two discs. A continuous pumping system was used, with one side pumping oxygen out and the other side pumping oxygen in. Tests were also conducted in the reverse direction. No change in EMF was noted when identical composition ZDY-2(YSZ) discs were used. However, when other YSZ discs were used (ZDY-4 [YSZ] and ZDY-2 [YSZ]), changes in EMF were noted which implied that ZDY-2(YSZ) discs have a higher ionic transference number. A relative ionic transference number of 0.998 was calculated. The calculation can be done as follows:

$$i_{leak}=\frac{4FV}{RT}\frac{\Delta pO_2}{t}$$

By knowing the cell volume, V and the supplying current i and by monitoring the EMF vs. time, we obtained the relative transference number, T_R, for the system;

$$T_R=(i-i_{leak})/i \tag{33}$$

At $pO_2\approx 10^{-3}$ atm, T_R (i.e., t_{CSZ}/t_{YSZ}) is 0.996, which indicates ZDT-4(YSZ) has a slightly higher ionic transferecne number.

In this particular case, we find that the iR drop for CSZ is higher than for YSZ. When the supplied current was stopped, the depolarization speed was much faster for YSZ. this suggests that YSZ would make a better oxygen pump.

2.4 Temperature effect on sealing cell

The temperature effect of mechanical pressure within

the cell on EMF must be taken into account because of the viscosity of Pyrex with temperature change. This effect can be explained in terms of the ideal gas law. Starting under the condition when EMF=0 (and assuming proper sealing), we can check the ideal gas behavior by varying the temperature and monitoring the EMF since no mass transport should occur, any change in EMF can be attributed to mechanical pressure. We obtain, EMF/T= A(ln T+B), where A=R/4F (the universal constant), and B $=\ln[n_{O_2} R/V_{cell} pO_2(ref)]$. The experimental data for a Pyrex-glass-sealed electrochemical cell in air showed the slope follows the universal constant, A, in the temperature range 820-940°C. However, above 1000°C a slight deviation from the theoretical line is seen.

3. Electrochemical transport measurement

Steady-state and non-steady-state electrochemical transport measurements can be made with the electrochemical cell shown in Fig. 1a. A steady-state flux is obtained by fixing the supplied current to the pumping electrolyte. When the EMF of the monitor electrolyte reaches a constant, steady-state is attained, i.e., $\partial EMF/\partial t = 0$. In this situation, the deviation from stoichiometry on both sides of the YSZ specimen will be in equilibrium with the respective surrounding gases. Fig. 2 shows the experimental steady-state oxygen flux versus log pO_2 at 950°C. Fig. 3a shows the steady-state oxygen flux versus log pO_2 for various temperatures for the reference pO_2 =0.003 atm, and Fig. 3b showed the different reference pO_2, 1.0, 0.003 and 1.0×10^{-14} atm. Fig. 4 shows the combined conductivity of ionic, and electronic (electron and hole) versus log pO_2 in YSZ.[2] Ionic conductivity is almost identical with total conductivity in the pO_2 range and temperatures. The minority conductivity, electron and hole conductivity, was calculated with Eqs 29 and 30.

For non-steady-state permeation measurement, pO_2 in the permeation cell was set equal to that outside of the cell for a sufficient time to ensure that the oxygen chemical potential across the cell was identical. This condition

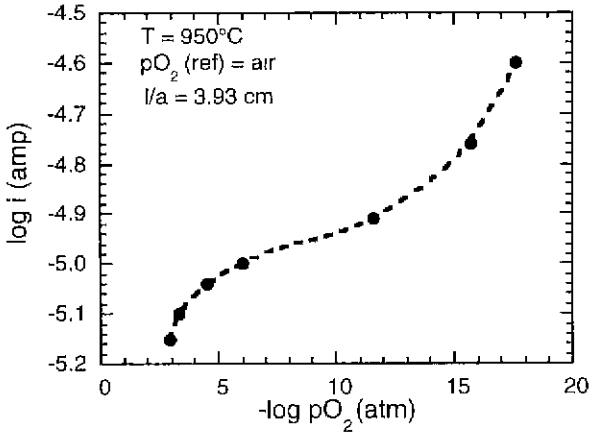

Fig. 2. Log of experimental steady-state current, i vs. log pO_2 (ref. pO_2=0.21 atm) at 950°C. Area/thickness=3.93 cm.

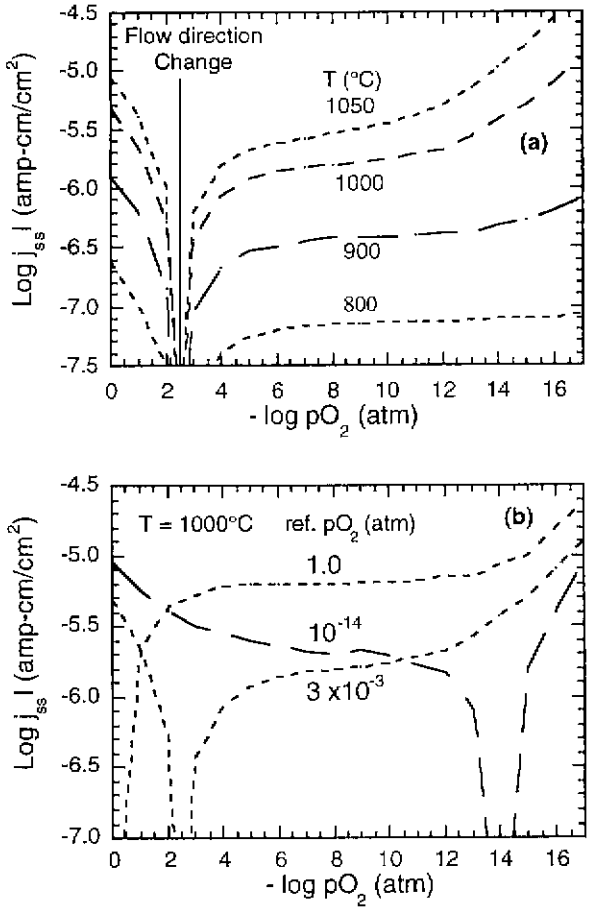

Fig. 3. (a) Log of steady-state oxygen flux, (j_{ss} l) in $Zr_{1-y}Y_yO_{2-(y/2)}$ vs. log pO_2 (reference $pO_2=3\times10^{-3}$ atm.) at 800-1050°C. (b) Log of steady-state oxygen flux, (j_{ss} · l) vs. log pO_2 reference pO_2=1.0, 3×10^{-3}, and 1×10^{-11} atm at 1000°C.

was established through pumping control or short-circuiting. Switching the reference gas to one much higher in oxygen partial pressure (e.g.,$<10^{-6}$ atm, switching to pure oxygen), initiates the non-steady-state condition. At the onset of the non-steady-state condition, we can record the change in pO_2 with time. After a given time period, the change in pO_2 will become constant, indicating pseudo-steady-state condition: The amount of oxygen diffused into the cell through the specimen also becomes a constant. At this time, the pO_2 in the cell is still orders of magnitude lower than the outside reference gas pO_2 of 1 atm. When this is true, we have met the boundary-condition requirements discussed in the theoretical analysis for Fick's second law.

Chemical diffusivity can be obtained from a plot of pO_2 vs. time. By repeating this experiment at different temperatures, we can obtain the chemical diffusivities and mobilities of the electrons and holes at various temperatures. From an analysis of an Arrhenius plot, the activation energy of the chemical diffusivity and the mobilities of the electronic or ionic species can be obtained. When we combine mobility with the electronic con-

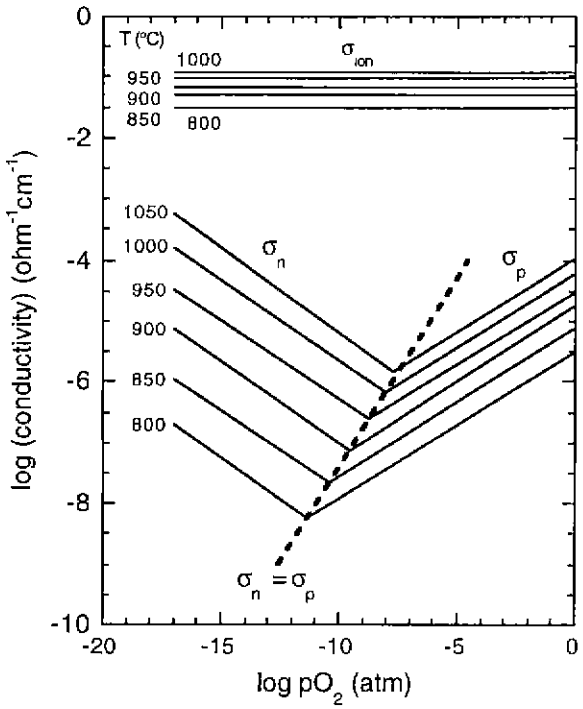

Fig. 4. Electron, hole and ionic conductivities vs. log pO_2 in YSZ.

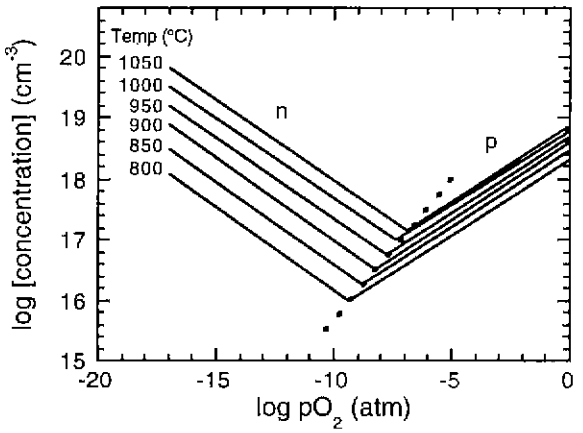

Fig. 5. Concentration of electrons and holes vs. log pO_2 in YSZ.

ductivity shown in Fig. 4 we can calculate the charge carrier concentration shown in Fig. 5. The narrow intervals (in Figs. 4 and 5) between temperatures are evident in the p-type region for both electrical conductivity and concentration at isobaric condition. This tells us that both the activation energy for electrons and formation energy are higher than those of the holes in the YSZ.

4. Constant composition study on CeO_{2-x}

Using a cell, Fig. 1b, we made simultaneous measurements of thermodynamic properties ($\Delta\bar{H}_{O_2}$ and $\Delta\bar{S}_{O_2}$) and electrical conductivity for constant compositions in nonstoichiometric metal oxides (MO_{2-x}). The solid-state coulometric titration cell for determining the deviation from stoichiometry has been described in previous papers.[2-4] Initially, the pO_2 was maintained the same inside and outside the system by creating a short circuit or by pumping oxygen. After the system was stabilized, some oxygen was pumped out at a fixed current for an appropriate time period to determine Δx, and the EMF was recorded. The procedure was repeated with different pO_2 levels and temperatures. A constant composition measurement could be attempted with the same setup as in the solid-state coulometric titration cell. The amount of oxygen transported during the measurement was assumed to be negligible compared to the variations of the deviation from stoichiometry, x. This condition is necessary because the thermodynamic properties are extracted at fixed compositions, as shown in Eq. 23. For large x values, the variation of x can be neglected in relationship to the amount of permeation of oxygen through the system during the measurement. To increase the value of x, oxygen was pumped out of the specimen; the current range for pumping was 200 to 600 μA. After the system stabilized, the EMF did not change with time during a period of 2 h (the EMF varies by 1 mV at 700 mV). An outside reference gas mixture of 1% O_2/Ar was used in an experiment in which the tem-

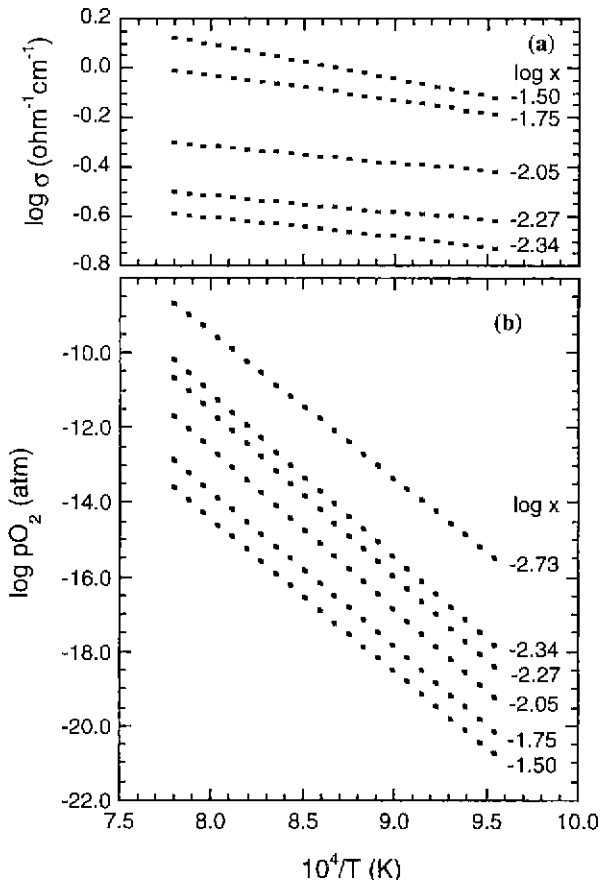

Fig. 6. Isocomposition data for conductivity (a) equilibrium pO_2 and (b) in CeO_{2-x}.

perature was varied.

Fig. 6 shows typical results of the simultaneous measurements of the temperature dependence of electrical conductivity (a) and equilibrium pO_2 (b) at various fixed values of x in CeO_{2-x}. These data were obtained for both cooling and heating cycles over the experimental temperature range that yielded reproducible data. Fig. 7a shows $\Delta\bar{H}_{O_2}$ (eV) calculated from the data of Fig. 6(b) using Eq (23), and Fig. 7b shows the electron migration energy, E_m (eV) obtained from the data of Fig. 6(a) using Eq (27). The values of $\Delta\bar{H}_{O_2}$ obtained from this study are about 0.1 eV lower than those of obtained by Panlener et al.[7] This difference in oxygen-formation enthalpy may arise from the difference in purity of the ceria specimens. Panlener et al. measured a 99.999% ceria sample, whereas in this

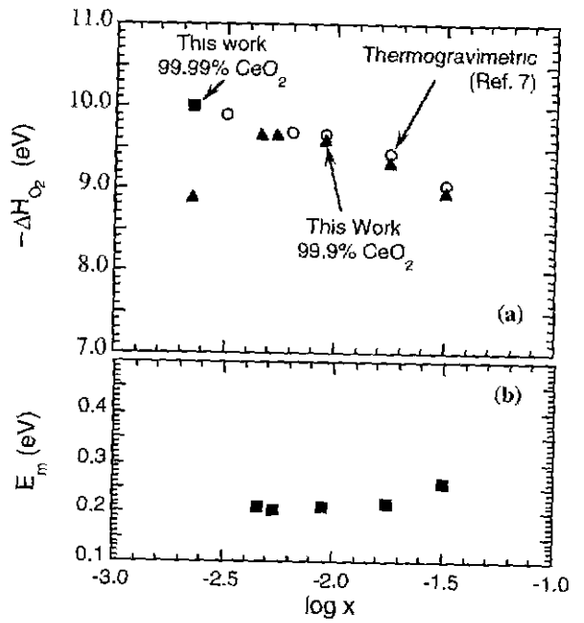

Fig. 7. Compositional dependence of partial molar enthalpy change, $\Delta\bar{H}_{O_2}$, (a) and migration energy for electrons (b) for CeO_{2-x}.

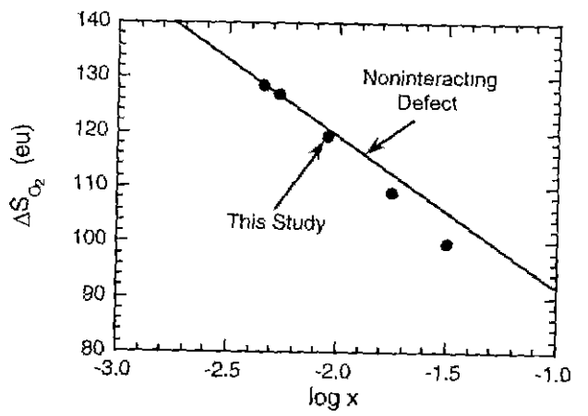

Fig. 8. Compositional dependence of $\Delta\bar{S}_{O_2}$ in CeO_{2-x}.

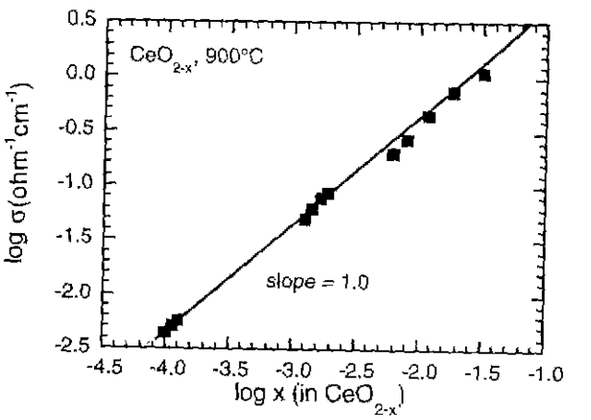

Fig. 9. Log σ vs. log x in CeO_{2-x} at 900°C for spontaneous pumping of oxygen in the range $10^{-4}<x<3.16\times10^{-2}$.

study we measured a 99.9% ceria sample. The 99.9% ceria contains 300 ppm of CaO as a major impurity. Ganier et al.[8] measured $\Delta\bar{H}_{O_2}$ for the CaO-doped CeO_2 system by employing a thermogravimetric measurement, their data show that $\Delta\bar{H}_{O_2}$ decreases as the CaO impurity in-

Table 1. Examples of Various Measurements Using Gas-tight Electrochemical Cells in Fig. 1

Cells	Sample	Measurements[a]	Ref.
Fig. 1a	YSZ	oxygen flux, j_{ss}, j_{nss} EMF	2
	$SrFeCo_{0.5}O_y$	oxygen flux, j_{ss}	13
	(CaO)-CeO_2	oxygen flux, j_{ss}, j_{nss} EMF	15
	(CaO/Ta_2O_5)-CeO_2	EMF	16
	$BaTiO_3$	oxygen flux, j_{ss} EMF	17
	Ag(Metallic Disk)	oxygen flux, j_{ss}, j_{nss}	18
Fig. 1b	CuO/Cu_2O	thermodynamic coulometric titration conductivity	19
	$YBa_2Cu_3O_y$	thermodynamic coulometric titration conductivity	25 26
	YSZ	thermodynamic coulometric titration (powder)	4
	$SrFeCo_{0.5}O_y$	conductivity	13,14
	10%CaO-CeO_2	coulometric titration (chunk sample)	20
	CeO_2	thermodynamic coulometric titration (conductivity sample)	21
	FeO	thermodynamic coulometric titration	27
	NiO	thermodynamic (chunk sample)	22
	Cr_2O_3	conductivity	23,24
Fig. 1c	SFC-II	Oxygen flux, j_{ss}	13

[a] j_{ss}=steady-state flux and j_{nss}=non-steady-state flux.

creases. This might be a reasonable explanation for our values of $\Delta\bar{H}_{O_2}$ being lower than those of Panlener et al. However 99.99% ceria, which (contains 200 ppm of CaO impurity) was also tested. The $\Delta\bar{H}_{O_2}$ was higher than in the 99.9% ceria sample, as shown in Fig. 7a. Fig. 8 shows the $\Delta\bar{S}_{O_2}$ vs. log x obtained from Fig. 6b of log pO_2 vs. 1/T at the intercept at 1/T=0 derived in Eq. 22.

In Fig. 7b, the migration energy for the electrons shows a slight increase with increasing x values. Fig. 9 shows the electrical conductivity increases with increasing x values. This provides direct evidence that pumping oxygen out produced electrons as a charge-compensating defect to the charged oxygen vacancies. Faber[28] used intense pulse neutron scattering method at Argonne National Laboratory to provide convincing evidence that the nonstoichiometric defects in CeO_{2-x} are oxygen vacancies. Table 1 shows examples of various measurements using the gas-tight electrochemical cells shown in Fig. 1.

III. Results and Discussions

Fig. 5 showed the combined hole and electron concentraion vs. log pO_2 (atm) for different temperatures.[2] The indicated concentrations for holes and electrons are comparable to those of other conventional metal-oxide systems such as CeO_{2-x},[3,7,8] NiO_{1+x}[22] etc., in this temperature and pO_2 region. But the mobilities of electrons and holes are much lower in YSZ. The ionic transference number, t_{ion}, is >0.99 and the material has a higher ionic conductivity. Consequently, the electronic transference number, t_{el} of 0.01, as well as the electronic conductivity is significantly lower than in other metal oxides. For YSZ, CSZ, etc., electronic conduction may be suppressed. In a good electrolyte, the mobile electronic carriers (electrons and holes) may be trapped on proper sites.

Now, we would like to discuss on the electronic hopping-type conduction in $Y_{0.148}Zr_{0.852}O_{1.926}$. When mobile electronic species are trapped on lattice sites, some useful Boltzman statistics for mobile electrons and holes may be applicable. Boltzman-type statistics are obeyed for the semiconducting properties of the ionic conductor 8 mole% Y_2O_3-ZrO_2, $Y_{0.148}Zr_{0.852}O_{1.926}$, at elevated temperatures (800-1050°C). Our analysis was carried out by combining the results from electronic transport[2] and solid-state coulometric titration measurements[4] under the assumption of trapping of electrons and holes on the appropriate sublattices. The results indicate that the transport of electrons and holes is due to thermal excitation process and that electrons and holes are obviously trapped on the appropriate sublattices.

Electrical conductivity for electrons, σ_n, and holes, σ_p, depends on the concentration, n for electrons and p, for holes, mobility, μ, and electronic charge, q, of the electronic defect. According to

$$\sigma_n = nq\mu_n \tag{34a}$$

and

$$\sigma_p = pq\mu_p, \tag{34b}$$

where μ_n, or μ_p shows a strong dependence on temperature, the transport can be treated by a hopping-type mechanism. If we assume that the mobilities do not depend on carrier concentration, conductivity varies with the concentration of electrons and holes. When the YSZ specimen is in equilibrium with oxygen at elevated temperatures, the oxygen is incorporated according to the reaction

$$\frac{1}{2}O_O^{\times} = \frac{1}{2}V_O^{\cdot\cdot} + \frac{1}{4}O_2(g) + e', \quad \Delta H_n^o$$

at low pO_2 (n-type region), or

$$\frac{1}{2}V_O^{\cdot\cdot} + \frac{1}{4}O_2(g) = \frac{1}{2}O_O^{x} + h^{\cdot}, \quad \Delta H_p^o$$

at high pO_2 (p-type region), where ΔH_n^o and ΔH_p^o are the reaction enthalpies of the proposed defect reactions at low and high pO_2, respectively. By the following assumptions,

(a) electrons and holes follow the ideal solution,

(b) n and p are negligible compared with the doping amount of yttrium, $[Y'_{Zr}]$, therefore we may put the electroneutrality as

(c) $[Y'_{Zr}] = 2[V_O^{\cdot\cdot}]$,

we then obtain the relations,

$$n = n_o \exp\left(-\frac{\Delta H_n^o}{kT}\right) pO_2^{-1/4} \tag{36a}$$

and

$$p = p_o \exp\left(-\frac{\Delta H_p^o}{kT}\right) pO_2^{+1/4} \tag{36b}$$

where n_o and p_o denote the pre-exponential constants.

Table 2 shows the model and empirical equations by combining the results of electronic transport[2,4] of conductivity and mobilities on the 8 mole% Y_2O_3-ZrO_2 sample. The carrier concentrations were calculated by combining equations for conductivity and mobility for each

Table 2. Electronic Mobilities and Conductivity in 8 mole% Y_2O_3-ZrO_2

Model Equations[a]		Empirical Equations[2]	
$\mu_n = \mu_n^o \mathrm{Exp}(-E_n/kT)$	(37a)	$\mu_n = 8.02\times10^2\mathrm{Exp}(-1.89/kT)$	(39)
$\mu_p = \mu_p^o \mathrm{Exp}(-E_p/kT)$	(37b)	$\mu_p = 0.85\mathrm{Exp}(-1.05/kT)$	(40)
$\sigma_n = \sigma_n^o \mathrm{Exp}(-Qn/kT)\, pO_2^{-1/4}$	(38a)	$\sigma_n = 1.31\times10^7\mathrm{Exp}(-3.88/kT)\, pO_2^{-1/4}$	(41)
$\sigma_p = \sigma_p^o \mathrm{Exp}(-Qp/kT)\, pO_2^{+1/4}$	(38b)	$\sigma_p = 2.35\times10^2\mathrm{Exp}(-1.67/kT)\, pO_2^{+1/4}$	(42)

[a]where, σ=conductivity ($ohm^{-1}cm^{-1}$), μ=mobility (cm^2/V sec), Q =activation energy (eV), E=migration energy (eV), and subscript n electrons and p holes. (Where k is the Boltzman constant, $k=8.614\times10^{-5}$ eV/deg)

type of electronic defect. For electrons,

$$n=\sigma_n/\mu_n q=(\sigma_n^\circ/\mu_n^\circ q)\exp(-\frac{Q_n-E_n}{kT})\,pO_2^{-1/4} \quad (43a)$$

and for holes,

$$p=\sigma_p/\mu_n q=(\sigma_p^\circ/\mu_p^\circ q)\exp(-\frac{Q_p-E_p}{kT})\,pO_2^{+1/4} \quad (43b)$$

The product of electronic defect concentrations gives

$$np=(\sigma_n\sigma_p/\mu_n\mu_p)/q^2$$
$$=[(\sigma_n^\circ\sigma_p^\circ/\mu_n^\circ\mu_p^\circ)/q^2]\exp(-\frac{Q_n+Q_p-E_n-E_p}{kT}), \quad (44a)$$

which has the form

$$np=N_cN_v\exp(-\frac{E_f}{kT}). \quad (44b)$$

Hence, the intrinsic carrier concentration is given by

$$n_i=\sqrt{np}=\sqrt{N_cN_v}\exp(-E_f/kT), \quad (45)$$

where E_f is the electron-hole pair formation energy, and N_c and N_v are the effective density of states for electrons and holes, respectively. By comparing Eqs. 44a and 44b, we obtain

$$E_f=Q_n+Q_p-E_n-E_p \quad (46)$$

and

$$N_cN_v=(\sigma_n^\circ/\mu_n^\circ q)(\sigma_p^\circ/\mu_p^\circ q) \quad (47)$$

Note that at pO_2=1.0 atm, the individual effective densities of state are given by; for electrons

$$N_c=(\sigma_n^\circ/\mu_n^\circ q) \quad (48)$$

and for holes

$$N_v=(\sigma_p^\circ/\mu_p^\circ q). \quad (49)$$

The effective densities of states of electrons and holes, N_c and N_v, in the fluorite cubic structure can be described in terms of the possible traping sites and lattice parameter, a_o:

$$N_v=\frac{4y}{a_o^3}(cm^{-3}), \quad (50)$$

in which we assumed that the hole is trapped at the yttrium location on one of the four possible zirconium sites in the unit cell of the $Zr_{1-y}Y_yO_{2-y/2}$. This gives a $(Y'_{Zr}\text{-}h^\cdot)^\circ$ complex. Similarly, for N_c,

$$N_c=\frac{4(1-y)}{a_o^3}(cm^{-3}), \quad (51)$$

where we assume the electrons to be trapped on one of the four possible normal zirconium sites forming a $(Zr_{Zr}^\times\text{-}e')'$ complex. Thus we obtain the following equation by the product of Eqs. 48 and 49 or 50 and 51,

$$N_cN_v=\frac{16y(1-y)}{a_o^6}=(\sigma_n^\circ/\mu_n^\circ q)(\sigma_p^\circ/\mu_p^\circ q) \quad (52)$$

We assumed that the electrons are trapped on the normal zirconium site as $(Zr_{Zr}^\times\text{-}e')'$. Because the electron mobility exhibited the behavior of a thermally activated process (5), the holes are also considered to be trapped on appropriate lattice sites. Here it is assumed that the hole is trapped at the yttrium ion on a zirconium site, i. e., $(Y'_{Zr}\text{-}h^\cdot)^\circ$; although there are several possible sites for holes-trapping in the lattice, only one may predominate, i.e., that with the strongest binding between holes and sites. Table 2 shows the effective density of states for holes (N_v) and for electrons (N_c) for the specimen. The calculated values for the experimentally obtained effective density of states for holes are 2.5 times lower than the values calculated from the lattice model. The effective density of states for electrons is 3.9 times higher than the values calculated from the lattice model. The agreement between the experimental and theoretical values is considered reasonable.

The hopping of electrons from one trapped site to another site occurs by thermal excitation. That is, the electron hops from one trapping zirconium site $(Zr_{Zr}^\times\text{-}e')'$ to a neighboring normal zirconium site, $Zr_{Zr}^\times$. Similarly, a hole hops from a hole trapped by yttrium on a zirconium site, $(Y'_{Zr}\text{-}h^\cdot)^\circ$ to normal yttrium on a zirconium site, Y'_{Zr}. The electron-hole pair formation energy, i.e., E_f=2.61 eV, is[2]

$$\frac{1}{2}O_O^\times\rightarrow\frac{1}{4}O_2(g)+\frac{1}{2}V_O^{\cdot\cdot}+e', \quad \Delta H_n^\circ=1.99eV$$

$$\frac{\frac{1}{2}V_O^{\cdot\cdot}+\frac{1}{4}O_2(g)\rightarrow\frac{1}{2}O_O^\times+h^\cdot, \quad \Delta H_p^\circ=0.62eV}{nil=e'+h^\cdot \qquad E_f=2.61eV}$$

The product of the effective density of states (N_vN_c) gives a value of 1.7×10^{44} cm^{-6} as calculated from the pre-exponential terms in the empirical equations and a value of 1.10×10^{44} cm^{-6} calculated from the lattice model (Table 3). The values for the electron-hole pair formation energy of 2.61 eV for experimental temperature range (850-1050°C) agrees reasonably well with the optical gap energy of 2.7-2.8 eV.[9] A slightly higher optical gap energy is expected according to the Frank-Condon principle, which states the optical gap energy is not lower than the thermal gap energy.[10] The temperature dependence of the indirect gap[9,11] can be represented by the linear re-

Table 3. Effective Density of States Calculated from Lattice model and from Empirical Equations for Holes (N_v) and Electrons (N_c) in 8 mole % Y_2O_3-ZrO_2 Specimen

	Effective Density of States	
	Lattice Model	Empirical Equations (pO_2=1.0 atm)
Holes $(Y'_{Zr}\text{-}h^\cdot)^\circ$	$4y/a_o^3$ $=4.36\times10^{21}$ cm^{-3}	$(\sigma_p^\circ/\mu_p^\circ q)pO_2^{+1/4}$ $=1.72\times10^{21}$ cm^{-3}
Electrons $(Zr_{Zr}^\times\text{-}e')$	$4(1-y)/a_o^3$ $=2.51\times10^{22}$ cm^{-3}	$(\sigma_n^\circ/\mu_n^\circ q)pO_2^{-1/4}$ $=9\ 89\times10^{22}$ cm^{-3}
N_vN_c	1.10×10^{44} cm^{-6}	1.71×10^{44} cm^{-6}
$\sqrt{N_vN_c}$	1.05×10^{22} cm^{-3}	1.31×10^{22} cm^{-3}

lationship as[9]

$$E_g(T) = 3.40 - 5.16 \times 10^{-4} T(K)\ (eV) \quad (53)$$

From the temperature dependence of the concentration of electrons and holes, a gap energy of 2.61 eV was determined over the temperature range 800-1000°C. In this temperature range, the values calculated from Eq. 53 are 2.7-2.8 eV, in close agreement with the values determined from the defect structure analysis in that laboratory.[12]

The value of directly obtaining partial molar thermodynamic quantities in the investigation of nonstoiciometric oxides is that it allows thermodynamic characterization without assuming a particular defect model. These quantities, which consist mainly of variations in oxygen chemical potential with changing temperature and composition, can best be used in support of, and in conjunction with, a proposed defect model. Together they provide insight, understanding, and a concise description of the nonstoichiometric behavior to develop various sensors,[29,30] membranes for gas separation/conversion for syngas generation,[31] to control oxygen contamination in the semiconductor and steel making industries, or for the wide range of environmental applications including the field of space development areas.

IV. Conclusions

By using a gas-tight electrochemical cell, we can perform high-temperature coulometric titration and measure electronic transport properties to determine the electronic defect structure of metal oxides. Based on cell design, both transport and thermodynamic measurements can be performed over a wide range of oxygen partial pressures. Our high-temperature gas-tight electrochemical cell are used to determine electronic defect structures and transport properties mainly for pure and doped-oxide systems, such as YSZ, and doped and pure ceria (Ca-CeO_2 and CeO_2).

Acknowledgment

This work has been supported by the U.S. Department of Energy, under Contract W-31-109-Eng-38.

References

1. T. Takahashi, Physics of Electrolytes, ed. J. Hladik, Academic Press, New York, 1972.
2. J.-H. Park and R. N. Blumenthal, "Electronic Transport in 8 Mole Percent Y_2O_3-ZrO_2", *J. Electrochem, Soc.*, **136**(10), 2867-2876 (1989)
3. J.-H. Park, "Thermodynamic and Conductivity Studies of Nonstoichiometric Cerium Dioxide by Coulometric Titration: a Simultaneous Measurement", *Physica B*, **150**, 80-85 (1988).
4. J.-H. Park and R. N. Blumenthal, "Thermodynamic Properties of Nostoichiometric Yttria-Stabilized Zirconia at Low Oxygen Pressures", *J. Am. Ceram. Soc.*, **72**(8) 1485-87 (1989).
5. H. Rickert, Electrochemistry of Solids, pp. 168-215 Springer-Verlag, Berlin, 1982.
6. L. Heyne, J. B Watchtman and A. D. Franklin., Mass Transport in Oxides, U.S. National Bureau of Standards Special Publication, 296, 1968.
7. R. J. Panlener, R. N. Blumenthal and J. E. Ganier, "A Thermodynamic Study of Nonstoichiometric Cerium Dioxide", *J. Phys. Chem. Solids*, **36**, 1213-1222 (1975).
8. J. E. Ganier, R. N. Blumenthal, R. J. Panlener and R. K. Sharma, "A Thermodynamic Study on CaO-doped Nonstoichiometric Cerium Dioxide", *J. Phys. Chem. Solids*, **37**, 369-378 (1976)
9. J.-H. Park and R. N. Blumenthal, "High-Temperature Optical Absorption Measurement of Single-Crystal, Yittria-Stabilized Zirconia", *J. Am Ceram. Soc.*, **71**(11) C-462-C-463 (1988).
10. A. J. Dekker, Solid State Physics, Englewood Cliff, Nj, Prentice Hall Inc., 1975.
11. R. H. Bube, Electronic Properties of Crystalline Solids, Academic Press, New York, 1974.
12. J.-H. Park, Electronic Conduction in Yttria Stabilized Zirconia, Ph. D. Dissertation, Marquette University, Milwaukee, WI (1985).
13. B. Ma, U. Balachandran, J.-H. Park and C. U. Segre, "Electrical Transport Properties and Defect Structure of $SrFeCo_{0.5}O_x$", *J. Electrochem. Soc.*, **143**(8), 1736-1744 (1996).
14. B. Ma, J.-H. Park and U. Balachandran, "Analysis of Oxygen Transport and Stoichiometry in Mixed-Conducting $SrFeCo_{0.5}O_x$ by Conductivity and Thermogravimetric Analysis", *J. Electrochem. Soc.*, **144**(8), 2816-2823 (1997).
15. M. A. Panhans and R. N. Blumenthal, "A Thermodynamic and Electrical Conductivity Study of Nonstoichiometric Cerium Dioxide", *Solid State Inoics.* **60**, 279-298 (1993).
16. E. K. Chang and R. N. Blumenthal, "A Thermodynamic and Electrical Conductivity Study of Nonstoichiometric Cerium Dioxide", *J. Solid State Chem.* **72**, 330-343 (1988).
17. E. T. Park and J.-H. Park, "Measurement of Oxygen Transport in $BaTiO_3$", unpublished results, Argonne National Laboratory (1997).
18. J.-H. Park, "Measuring Oxygen Diffusivity and Solubility in Solid Silver with a Gas-Tight Electrochemical Cell", *Mat. Lett.*, **9**(9) 313-316 (1990).
19. J.-H. Park and K. Natesan, "Oxidation of Copper and Electronic Transport in Copper Oxides", *Oxid. Met.*, **39**(5-6), 411-435 (1993)
20. J.-H. Park, R. N. Blumenthal and M. A, Panhans, "Direct Measurement of Thermodynamic Properties in Nonstoichiometric CaO-Doped Cerium Dioxide by Coulometric Titration", *J. Electrochem, Soc.*, **135**(4), 855-859 (1988).
21. M. A. Panhans and R. N. Blumenthal, "A Thermodynamic and Electrical Conductivity Study of Nonstoichiometric Cerium Dioxde", **60**, 279-298 (1993).
22. Y. D. Tretyakov and R. A. Rapp, "Nonstoichiometries

and Defect Structures in Pure Nickel Oxide and Lithium Ferrite", *Trans. Metall. Soc.*, (AIME) **245**, 1235-1241 (1969).
23. J.-H. Park and K. Natesan, "Electronic Transport in Thermally Grown Cr_2O_3", *Oxid. Met.*, **33**(1-2), 31-54 (1990).
24. J.-H. Park, K. Natesan and D. L. Rink, "Sulfur and Oxygen Transport Properties of Thermally Grown Cr_2O_3 Films", *High Temperature Science*, **30**, 193-219 (1991).
25. J.-H. Park and P. Kostic, "Conduction Mechanisms and Phase Transformations in $YBa_2Cu_3O_y(6.1<y<7.0)$", *Mat. Lett.*, **6**(10), 327-330 (1988).
26. J.-H. Park, P. Kostic and J. P. Singh, "Electrical Conductivity and Chemical Diffusion in Sintered $YBa_2Cu_3O_y$", *Mat. Lett.*, **6**(11-12) 393-397 (1988).
27. R. A. Giddings and R. S Gordon, "Solid State Coulometric Titration: Critical Analysis and Application to Wustite", *Jelectrochem. Soc.*, **121** 793-799 (1974).
28. J. Faber, Jr, "High-Temperature Charge-Density Studied of CeO_{2-x} Using X-ray and Neutron Diffaction Techniques", *Physica B*, **150**, 241-249 (1988).
29. D. R. Baker and M. W. Verbrugge, "Theory and Simulation of Solid-Electrolyte Wide-Range Sensors for Combustion-Gas Streams", *J. Electrochem. Soc.*, **143**(7), 2396-2409 (1996).
30. M. W. Verbrugge and D. W. Dees, "Theoretical Analysis of a Blocking-Electrode Oxygen Sensor for Combustion-Gas Streams", *J. Electrochem. Soc.*, **140**(7), 2001-2010 (1993).
31. U Balanchandran, J. T. Dusek, S. M. Sweeney, R. B. Poeppel, R. L. Mieville, P. S. Maiya, M. S. Kleefisch, S. Pei, T. P. Kobylinski, C. A. Udovich and A. C. Bose, "Methane to Syngas via Ceramic Membranes", *Am. Ceram. Soc. Bull.* **74**(1), 71-75 (1995),